Microstructure and high cycle fatigue fracture surface of a Ti-5Al-5Mo-5V-1Cr-1Fe titanium alloy

Wu, G. Q., Shi, C. L., Sha, W., Sha, A. X., & Jiang, H. R. (2013). Microstructure and high cycle fatigue fracture surface of a Ti-5Al-5Mo-5V-1Cr-1Fe titanium alloy. *Materials Science and Engineering A*, *575*, 111–118. https://doi.org/10.1016/j.msea.2013.03.047

Published in:
Materials Science and Engineering A

Document Version:
Peer reviewed version

Microstructure and high cycle fatigue fracture surface of a Ti-5Al-5Mo-5V-1Cr-1Fe titanium alloy

G.Q. Wu[1,*], C.L. Shi[1], W. Sha[2], A.X. Sha[3], H.R. Jiang[1]

[1]School of Materials Science and Engineering, Beihang University, 37 Xueyuan Road, Haidian District, Beijing 100191, China

[2]School of Planning, Architecture and Civil Engineering, Queen's University Belfast, Belfast BT7 1NN, UK

[3]Beijing Institute of Aeronautical Materials, Beijing 100095, China

*Corresponding author: Tel: +86 1082313240; E-mail: guoqingwu@buaa.edu.cn

Abstract

Because of the requirements for the damage tolerance and fatigue life of commercial aircraft components, the high cycle fatigue (HCF) properties of Ti-5Al-5Mo-5V-1Cr-1Fe titanium alloy forgings are important. The effects of microstructure types of the α + β titanium alloy on fatigue properties need to be understood. In this paper, by analysing the fracture surfaces of the titanium alloy having four types of microstructure, the effects of microstructure are investigated. The differences of initiation areas and crack propagation among different microstructures were studied. It was found that the area of the initiation region decreases in the order of coarse basketweave, fine basketweave, Widmanstätten, and bimodal microstructure.

Keywords: titanium alloy; bimodal microstructure; lamellar microstructure; basketweave microstructure; high cycle fatigue; initiation region

1. Introduction

In the Ti-5Al-5Mo-5V-1Cr-1Fe titanium alloy, different types of microstructure can be obtained after different heat treatments, such as bimodal, equiaxed, and Widmanstätten [1,2]. Literature reports show that different microstructures can lead to different mechanical properties such as strength, ductility, and fatigue properties. The Ti-5Al-5Mo-5V-1Cr-1Fe titanium alloy is a structural material designed based on considerations of damage tolerance targets, so its fatigue properties have attracted wide attention [3-5]. On the influence of microstructure on the fatigue properties of titanium alloys, current research has concentrated on the characteristics of low cycle fatigue of different microstructures, and fracture surface analysis of crack propagation rate and crack initiation [6,7]. Judging from the majority of the literature, in general, materials having high yield strength would have high fatigue strength as well [8,9]. For the Ti-5Al-5Mo-5V-1Cr-1Fe titanium alloy with similar yield strength levels but different microstructure, there is a lack of detailed research on its fatigue properties.

At present, there is no universal criterion or standard to define the initiation period of cracks. Usually, cracks having a length of 0.05-0.1 mm are regarded as the nucleus cracks under fatigue. The corresponding cycles are crack initiation periods, their length determined by the stress levels. Under low stress, fatigue crack initiation period can be more than half of the entire life. Many experiments have proved that, for aerospace aluminium alloys, the vast majority of their fatigue life, 80-90%, is spent on the propagation of initially minute cracks, starting at 10-20 micrometres, to long cracks [10]. Microstructure has large influences on the initiation and fracture (tertiary) periods of high cycle fatigue cracks, but has much smaller influence on the crack propagation period. As the fracture period is only a very small fraction of the high cycle fatigue life, studying the effect of microstructure on the initiation of high cycle fatigue becomes the most important.

Studies of the stable propagation mechanisms of small cracks and long cracks are rather mature, as are studies of surface crack initiation mechanisms during low cycle fatigue under high stress or strain [11]. However, there is no consensus on the initiation mechanism under low stress, high cycle conditions. Research on initiation mechanism has been carried out from different directions. Przybyla et al. [12] and Marines-Garcia et al. [13] believe that the internal initiation mechanism is related to the internal defects made during the alloy making process. Chan and Lee [14-16] studied the crack initiation mechanism by analysing the different stress on two phases in bimodal structure during the fatigue loading process. Oguma and coworkers [9,17-18] studied the grain size, internal initiation area, and internal and external fatigue crack initiation, by carrying out high cycle fatigue experiments in vacuum and air, in attempts to evaluate the mechanism of internal initiation. In addition, a mechanism relating high cycle fatigue to internal slip bands has been proposed. Also, cyclic loading may induce the formation and propagation of defects through the irreversible movement of atoms under thermal agitation, causing stress concentration at internal defects leading to fatigue crack initiation. Initiation period is critical to high cycle fatigue properties. Manually defining the initiation period, as used in the past and now, using a measurable length, obviously cannot satisfy further research on crack initiation. There is ample recent literature describing specific mechanisms of crack initiation and crack propagation [19-23].

Observation and characterisation have been made, to compare and analyse the microstructure of the Ti-5Al-5Mo-5V-1Cr-1Fe titanium alloy, with different microstructure types, before and after fatigue. No obvious changes after high cycle fatigue, nearly 10^7 cycles, have been found in microstructure, using both optical metallography and scanning electron microscopy (SEM), with magnifications ranging from low magnification to 20,000 times.

In published literature, there have been studies of the general mechanical properties of the Ti-5Al-5Mo-5V-1Cr-1Fe titanium alloy. With increasing application range of this alloy, it is important to understand its fatigue properties, but there has been virtually no literature on

these internationally. The objective of this work is to reveal the different effects of different microstructure types on crack initiation and propagation during high cycle fatigue process of the Ti-5Al-5Mo-5V-1Cr-1Fe titanium alloy. The aim is to provide a reference point for the optimisation of the alloy processing parameters for achieving better high cycle fatigue performance. In this paper, different microstructural types are analysed quantitatively and in association with their composition characteristics. Based on high cycle fatigue failure experiments of four types of microstructure, fatigue fracture surfaces are analysed, to evaluate the effect of different microstructures on the initiation and propagation periods during the fatigue fracture process.

2. Experimental material and method

The forged Ti-5Al-5Mo-5V-1Cr-1Fe titanium alloy studied in this paper was provided by Beijing Institute of Aeronautical Materials. Its chemical composition is shown in Table 1 and mechanical properties in Table 2. The processing parameters for the four types of structure were different and undisclosed. Heat treatment processes, however, were all typical double annealing. For the bimodal structure, air cooling was used after forging in the two-phase region, nearer to the upper temperature limit. Widmanstätten structure was achieved through air cooling after forging in single phase region. The two basketweave structures were achieved by air cooling after deformation near the phase transformation point.

Table 1. Chemical composition of Ti-5Al-5Mo-5V-1Cr-1Fe titanium alloy (wt.%)

C	V	Fe	Al	N	H	O	Mo	Cr	Ti
0.021	5.06	0.98	5.10	0.02	0.003	0.15	5.14	0.93	balance

Fatigue experiments were carried out on a high frequency fatigue facility. Loading stress ratio was 0.06, frequency 120 Hz. The dimensions of the fatigue specimen are shown in Fig. 1, having a minimum diameter of 5 mm.

Table 2. Mechanical properties of Ti-5Al-5Mo-5V-1Cr-1Fe titanium alloy with different types of microstructure

Type	0.2 proof strength (MPa)	Tensile strength (MPa)	Elongation (%)	Reduction of area (%)	Fatigue strength at 10^7 cycles (MPa)
Bimodal	1197	1215	14	56	880
Widmanstätten (lamellar)	1180	1199	5	9	780
Coarse basketweave	1093	1133	14	39	650
Fine basketweave	1084	1141	15	36	730

Scanning electron microscopy was carried out on JSM-5800 and Zeiss Ultra 55 machines, of the microstructure of the Ti-5Al-5Mo-5V-1Cr-1Fe titanium alloy and its fatigue fracture surface morphology. Composition analysis of different microstructural components was made using the Zeiss Ultra 55 microscope. The Kroll's etchant was used, with 3%HNO_3 and 1% HF, in water.

The size of microstructural features was quantitatively measured using the Nano Measurer 1.2 software, including the grain size of primary α phase in the bimodal structure, in both transverse and longitudinal directions, the width of grain boundary and grain interior α in Widmanstätten and fine basketweave structures, and α size in transverse and longitudinal directions in the coarse basketweave structure. Quantitative measurements were made by using five photos, to make sure that there were more than 100 measurements in virtually all cases.

3. Results and discussion

3.1. Microstructural characteristics and phase composition

Four types of microstructure were obtained from the alloy after different hot processing and heat treatments (Figs. 2-5). As shown in Fig. 2, in the bimodal structure, the primary α phase is equiaxed and uniformly distributed. Its average grain size is 1.3 μm, calculated based on 593 measurements, range 0.4-3.6 μm (Fig. 2b). The length along the long direction of the grains is 3.5 μm, based on 107 measurements, range 2.4-5.1 μm. Because the primary α phase, precipitated during recrystallisation, is on β grain boundaries and interior, β grains are not visible in the micrograph.

Fig. 3a shows clear, coarse β grains, and the Widmanstätten microstructure under the optical microscope. Under the magnification used in Fig. 3b, the main characteristics of the

Widmanstätten microstructure are as follows. On the grain boundaries of coarse β grains, there is coarse grain boundary α phase, with average width 1.7 μm (108 data points, range 1.2-2.8 μm, Fig. 3e). Along grain boundary regions, narrow α plates extend into the grains in both sides, or just in one side. Sometimes, they do not appear as arrays, extending into the grains. In the interior of β grains, fine α plates appear in weaving patterns, average plate thickness 0.5 μm (328 data points, range 0.2-1.2 μm, Fig. 3f). Inside grains, in certain regions, large quantities of lathy α particles appear, average dimension 4.2 μm (range 2.8-7.1 μm). Under the higher magnification in Fig. 3d, in the β matrix near the grain boundaries or inside the grains, there are large quantities of needle shape α precipitates. The volume fraction of α is about 53%.

Under low magnification, the fine basketweave structure includes β grains having elongated to spheroidal shapes. Fig. 4a shows grain boundary α phase, more discontinued with uneven width compared to the grain boundary phase in the Widmanstätten microstructure, average width 1.6 μm (148 data points, range 0.5-2.8 μm). The average width of narrow α plates inside grains is 0.7 μm (469 data points, range 0.3-1.7 μm, Fig. 4c).

Fig. 5 shows the non-uniform coarse basketweave structure, average α phase dimension 1.7 μm (309 data points, range 0.4-3.4 μm, Fig. 5b). The average length is 5.0 μm (74 data points, range 3.1-16.0 μm). The α phase morphology includes equiaxed, plate (maximum aspect ratio 6.8), as well as the discontinuous grain boundary phase.

From these quantitative results, there are similarities in the characteristics in the bimodal, coarse basketweave, fine basketweave, and Widmanstätten structures. Comparison shows that the average α grain size in the coarse basketweave structure is larger than in the bimodal structure, with much larger length. The thickness of the grain boundary α phase in the Widmanstätten microstructure is larger than in the fine basketweave structure, but the thickness of the α plates inside grains is smaller.

Table 3 shows composition analysis results using energy dispersive analysis of the four types of microstructure. Each data is the average of three measurements.

Table 3. Mass percentage of alloying elements in different microstructures in Ti-5Al-5Mo-5V-1Cr-1Fe titanium alloy

Microstructure	Phase	Al	V	Mo	Fe	Cr
Bimodal	α	7.1	2.0	1.7	0.2	0.3
	β	4.5	6.0	8.0	1.4	1.3
Widmanstätten	Grain interior α	5.3	4.2	4.6	0.9	0.7
	Grain boundary α	6.5	2.0	1.7	0.2	0.3
	β	4.8	5.2	6.6	1.2	1.1
Fine basketweave	Grain interior α	5.8	2.9	2.8	0.5	0.3
	Grain boundary α	5.6	4.0	4.1	0.8	0.7
	β	4.3	5.4	7.2	1.4	1.1
Coarse basketweave	α	6.1	2.3	2.0	0.3	0.3
	β	4.1	6.2	7.7	1.4	1.4

There is a relationship between the alloy strength improvement over pure titanium and alloying contents, though it is somewhat empirical. The total strengthening in a titanium alloy is the sum of strengthening due to substitutional elements and interstitial elements. Solid solution strengthening is determined by the difference in elastic modulus and the atom size of the interacting elements.

3.2. High cycle fatigue fracture surface analysis of different types of microstructure

With decreasing fatigue loading, previous testing results [17,19] showed that the fatigue crack initiation location moved from surface to sub-surface. S-N curves were given in a previous publication [24] and so will not be repeated here.

Fig. 6 gives macroscopic scanning electron micrographs of the Ti-5Al-5Mo-5V-1Cr-1Fe titanium alloy having a coarse basketweave structure, under two different cyclic loading. As seen from the two fractographs, the large propagation regions are relatively flat, but the final instantaneous fracture regions are not. This is because of the increased stress during the final instantaneous fracture period. Judging by the reversal of the spreading direction, the fatigue fracture crack initiation location can be obtained. In the coarse basketweave structure, the initiation was on the surface under the loading of 875 MPa, but it moved to sub-surface under the loading of 625 MPa.

3.2.1. Initiation area

Apart from the fatigue fracture surfaces of this type of specimens, this section studies the fatigue fracture surfaces of all four types of structure in the Ti-5Al-5Mo-5V-1Cr-1Fe titanium alloy. All results show that with decreasing fatigue loading, the fatigue fracture initiation location moves from surface to sub-surface. This phenomenon does not depend on structure type.

Crack initiation region, in Figs. 7c, 8c, 9b and 10b, is defined as the area on the fracture surface that is flat and shows no sign of streaky contour that spreads to all directions, i.e., around 360°, away from the region. Such feature of the spreading streaky contour results from the crack growth, and the crack initiation regions are inside, in the SEM pictures, the

crack growth regions. Crack initiation regions are formed before the cracks start to spread, in the crack growth regions.

Fig. 7 shows fracture surface and initiation region morphological characteristics of bimodal structure after high cycle fatigue (840 MPa loading, life 4.4×10^6). From Fig. 7a, large areas in this fracture surface are flat fatigue crack propagation zone, but the instantaneous fracture region has a typical shear fracture characteristic. Combining with the reversal of the crack propagation direction in Fig. 7b and the high magnification secondary electron image in Fig. 7c, we can see that the initiation area is sub-surface, in the bimodal structure under high cycle loading. The initiation area is about 200 μm^2. This initiation area is rather flat, and the nearby area surrounding the initiation consists of large quantities of discontinuous coarse α grains. This is consistent with the characteristics of this type of structure. Forging at two-phase temperatures (near the higher end) and subsequent heat treatment causes recrystallisation, at grain boundaries and grain interior. Due to the processing and recrystallisation, the grain boundary α phase becomes discontinuous.

From the macrograph of Fig. 8a showing the entire fracture surface of the high cycle fatigue fracture of Widmanstätten structure (loading 800 MPa, life 7.7×10^6), it can be seen that the large propagation regions have a typical intergranular fracture characteristic, related to the coarse β grains of this structure. This reflects the resistance to stable propagation of long cracks of this structure. Fig. 8b, on the other hand, is a scanning micrograph of the initiation area under a relatively high magnification. Judging from the reversal of bright spreading directions all round, the fatigue crack initiation region is sub-surface, at the centre of the spreading lines. From Fig. 8c, the biggest characteristic of the initiation area is that it locates at a triple grain junction of three grains. If we use the region where the spreading lines reverse directions and disappear as the fatigue crack initiation region, measurement showed that the area is 1300 μm^2. The characteristic structure of the initiation includes coarse β grain boundary α phase, and α plate arrays along grain boundaries and inside grains. These arrays

have similar crystallographic orientations. Triple grain junctions are favoured locations for fatigue crack initiation. During its formation, the initiation area was not limited to grain boundaries, resulting in increased initiation area.

Fig. 9a is a macrograph showing high cycle fatigue fracture surface of the fine basketweave structure (loading 720 MPa, life 7.1×10^6). It can be seen that the instantaneous fracture region occupies about half of the fracture area, and it is not flat at all, indicating large plastic deformation during the instantaneous fracture. At the transition from propagation to instantaneous fracture, there are large quantities of secondary cracks. Judging by the crack propagation direction reversion in the relatively flat region, it can be found that the crack initiation located sub-surface of the fatigue specimen. This was the case in two high cycle fatigue fracture surfaces observed of this microstructure. The initiation structure shown in Fig. 9b consists of bunches of coarse lathy α phase, distributed in a nearly array form, together with fine α plate arrays surrounding them. The measured initiation area is about 1800 μm^2.

Fig. 10 shows the low and high magnification initiation area of the coarse basketweave structure, at high cycle fatigue (loading 625 MPa, life 9.1×10^6). It can be seen that the initiation area is still closely related to grain boundaries. The measured initiation area size is about 2500 μm^2.

The above results show that, in the Ti-5Al-5Mo-5V-1Cr-1Fe titanium alloy, after nearly 10^7 loading cycles leading to fatigue failure, the area of initiation regions in the fatigue fracture surface is different for different microstructure types. This is in the decreasing order of coarse basketweave, fine basketweave, Widmanstätten, and bimodal. Higher fracture strength corresponds to smaller initiation area.

3.2.2. Propagation region

Fig. 11 shows the morphology characteristics of stable propagation regions in the fracture surface of the Ti-5Al-5Mo-5V-1Cr-1Fe titanium alloy having four different microstructure types (load cycle nearly 10^7). The common feature is the fatigue bands in the stable propagation regions, which are more obvious in the blocky α phase in bimodal and coarse basketweave structures and less obvious in the other two types of structure, probably due to the small α plate thickness in their grains. This morphological feature shows that the stable propagation period in all four microstructural types is associated with plastic deformation. The different structural types have some influences on this region in the fracture surface, but it is hard to clarify how such influences affect the overall fatigue properties. If, in future work, the strength characteristics of each phase in the different structures can be measured, using, for example, atomic force microscopy and nanoindentation, the effects of different microstructural types and structural parameters on the stable propagation of fatigue cracks may be understood and quantified.

How the different microstructures result in different values of fatigue strength and the mechanism in each case are the subject of a very recently published paper by the authors [25]. Thus, these will not be repeated here and Ref. [25] should be referred to.

4. Conclusions

Characteristics of Widmanstätten, bimodal and basketweave microstructures, with similar yield strength, have been studied. Fatigue fracture initiation and propagation regions have been compared, under high cycle fatigue conditions, after nearly 10^7 loading cycles. The main findings are as follows.

(1) There exists obvious grain boundary phase in the Widmanstätten and fine basketweave microstructures. The grain boundary α phase in Widmanstätten structure is thicker. There is no obvious difference in the β phase in the four structural types. The thickness of the grain interior α phase decreases in the order of coarse basketweave, bimodal, fine basketweave, and Widmanstätten.

(2) The high cycle fatigue initiation is at sub-surface, in the Ti-5Al-5Mo-5V-1Cr-1Fe titanium alloy having four microstructure types, compared to initiation at surface at higher stresses. The area of the initiation region decreases in the order of coarse basketweave, fine basketweave, Widmanstätten, and bimodal. Structural types with higher fatigue strength correspond to smaller initiation area. No obvious difference was found in the high cycle fatigue propagation regions among the four microstructure types.

References

[1] G. Lütjering, J.C. Williams, Titanium, Springer, Hamburg, 2007, pp. 234-238.

[2] L.M. Orlova, A.D. Lemesh, G.P. Belozub, T.V. Filatova, Met. Sci. Heat Treat. 28 (1) (1986) 73-77.

[3] J. Zhang, X. Cheng, Z. Li, Mater. Des. 31 (2010) 4329-4335.

[4] C. Leyens, M. Peters, Titanium and Titanium Alloys, Wiley-VCH, Weinheim, 2003, pp. 140-145.

[5] H. Knobbe, P. Koter, H. Christ, C.P. Fritzen, M. Riedler, Procedia Eng. 2 (2010) 931-940.

[6] P.J. Golden, R. John, W.J. Porter III, Int. J. Fatigue 31 (2009) 1764-1770.

[7] A.J. McEvily, T. Nakamura, H. Oguma, K. Yamashita, H. Matsunaga, M. Endo, Scr. Mater. 59 (2008) 1207-1209.

[8] J.H. Zuo, Z.G. Wang, E.H. Han, Mater. Sci. Eng. A 473 (2008) 147-152.

[9] H. Oguma, T. Nakamura, in: G. Lütjering, J. Albrecht (Eds.), Ti-2003 Science and Technology, Wiley-VCH, Weinheim, 2004, pp. 1783-1790.

[10] K.N. Shivakumar, P.W. Tan, J.C. Newman, Int. J. Fract. 36 (3) (1988) 43-50.

[11] J. Schijve, Fatigue of Structures and Materials, second ed., Springer, Delft, 2009, pp. 13-14.

[12] C. Przybyla, R. Prasannavenkatesan, N. Salajegheh, D.L. McDowell, Int. J. Fatigue, 32 (2010) 512-525.

[13] I. Marines-Garcia, P.C. Paris, H. Tada, C. Bathias, Mater. Sci. Eng. A, 468-470 (2007) 120-28.

[14] K.S. Chan, Y.D. Lee, Metall. Mater. Trans. A 39 (2008) 1665-1675.

[15] K.S. Chan, Int. J. Fatigue 32 (2010) 1428-1447.

[16] K.S. Chan, Int. J. Fatigue 32 (2010) 526-534.

[17] H. Oguma, T. Nakamura, Scr. Mater. 63 (2010) 32-34.

[18] T. Nakanura, H. Oguma, T. Shiina, in: G. Lütjering, J. Albrecht (Eds.), Ti-2003 Science and Technology, Wiley-VCH, Weinheim, 2004, pp. 1775-1782.

[19] Z. Huang, D. Wagner, C. Bathias, P.C. Paris, Acta Mater. 58 (2010) 6046-6054.

[20] K.H. Nam, I.H. Park, S.H. Ko, Nature 485 (2012) 221–224.

[21] S.E. Stanzl-Tschegg, B. Schönbauer, Int. J. Fatigue 32 (2010) 886–893.

[22] A.K.M. Iqbal, Y. Arai, W. Araki, Mater. Des. 45 (2012) 241-252.

[23] B.L. Josefson, J.W. Ringsberg, Int. J. Fatigue 31 (2009) 1413-1421.

[24] C. Shi, G. Wu, A. Sha, H. Jiang, Procedia Eng. 27 (2012) 1209-1215.

[25] G.Q. Wu, C.L. Shi, W. Sha, A.X. Sha, H.R. Jiang, Mater. Des. 46 (2013) 668-674.

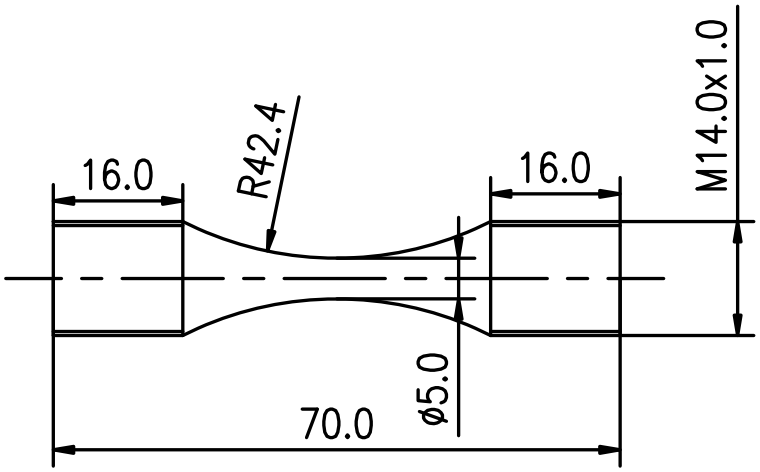

Fig. 1. Dimensions of fatigue specimen.

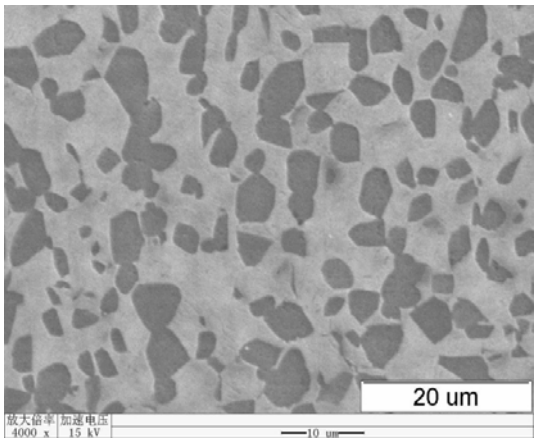

(a)

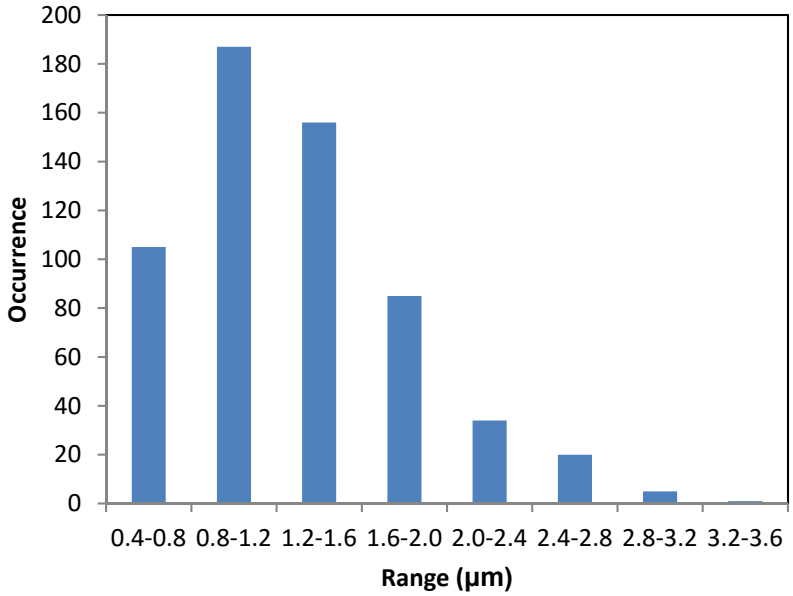

(b)

Fig. 2. (a) Bimodal microstructure in Ti-5Al-5Mo-5V-1Cr-1Fe titanium alloy, by SEM; (b) grain size histogram.

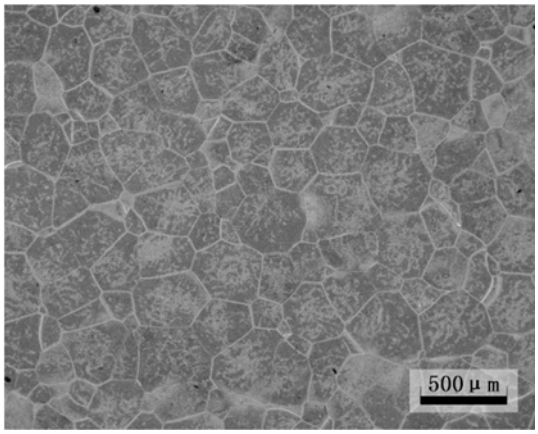
500 μ m

(a)

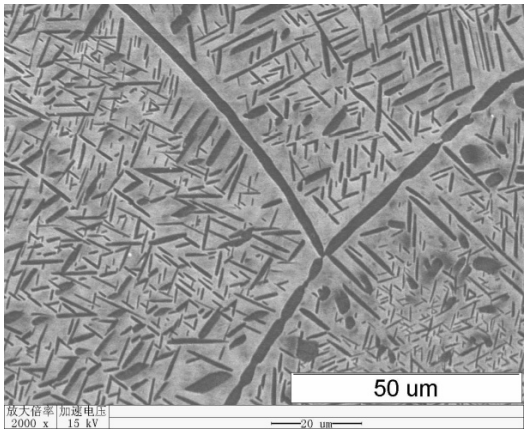
50 um
放大倍率 加速电压
2000 x 15 kV
20 um

(b)

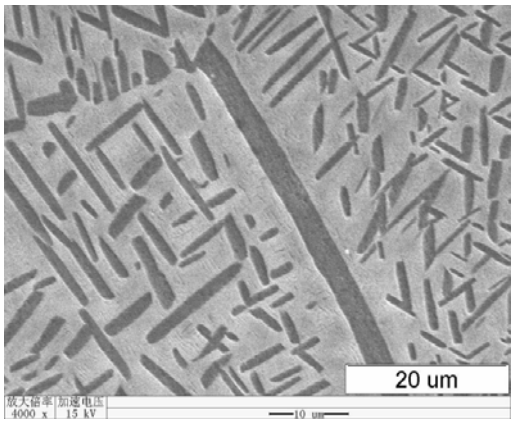
20 um
放大倍率 加速电压
4000 x 15 kV
10 um

(c)

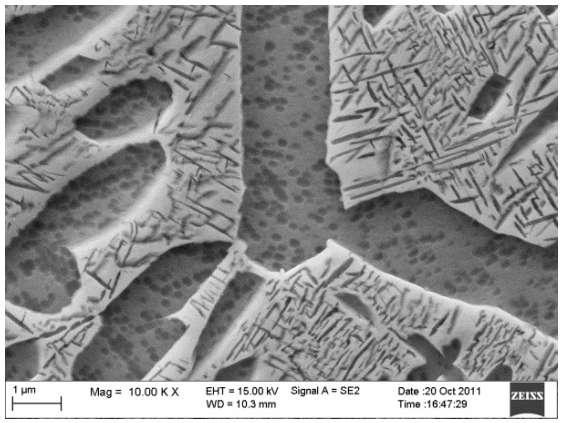
1 μm
Mag = 10.00 K X
EHT = 15.00 kV
WD = 10.3 mm
Signal A = SE2
Date :20 Oct 2011
Time :16:47:29
ZEISS

(d)

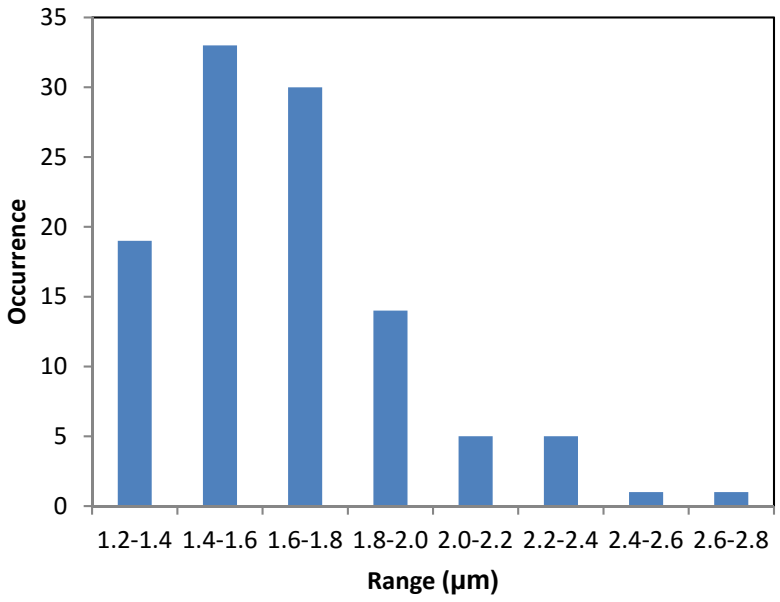
35
30
25
20
15
10
5
0
Occurrence
1.2-1.4
1.4-1.6
1.6-1.8
1.8-2.0
2.0-2.2
2.2-2.4
2.4-2.6
2.6-2.8
Range (μm)

(e)

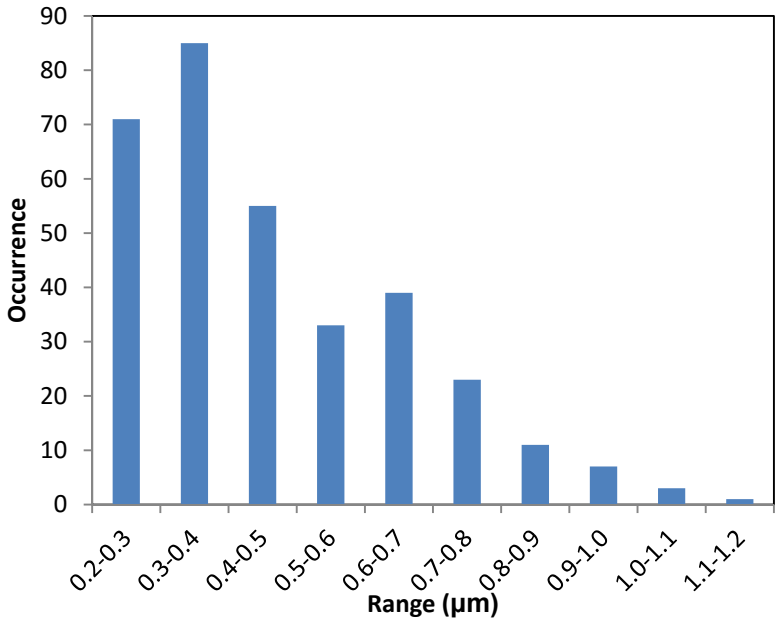

(f)

Fig. 3. Widmanstätten lamellar microstructure in Ti-5Al-5Mo-5V-1Cr-1Fe titanium alloy. (a) Low magnification optical micrograph; (b,c) relatively high magnification SEM; (d) high magnification grain boundary microstructure by SEM; (e) coarse grain boundary α phase width histogram; (f) β grains interior α plates thickness histogram.

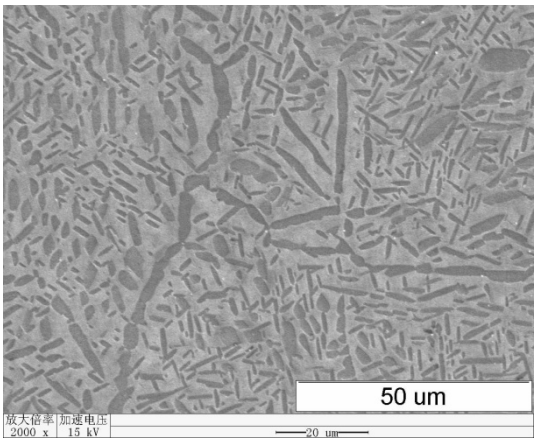

(a)

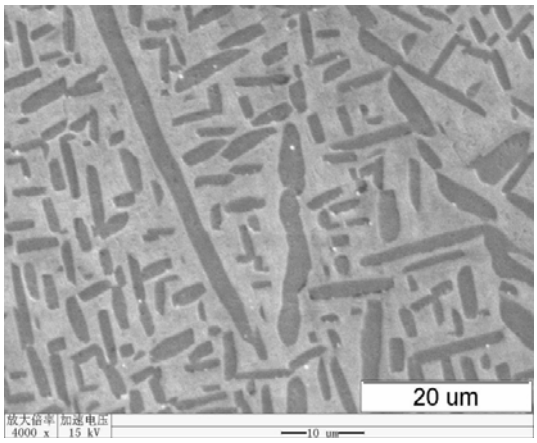

(b)

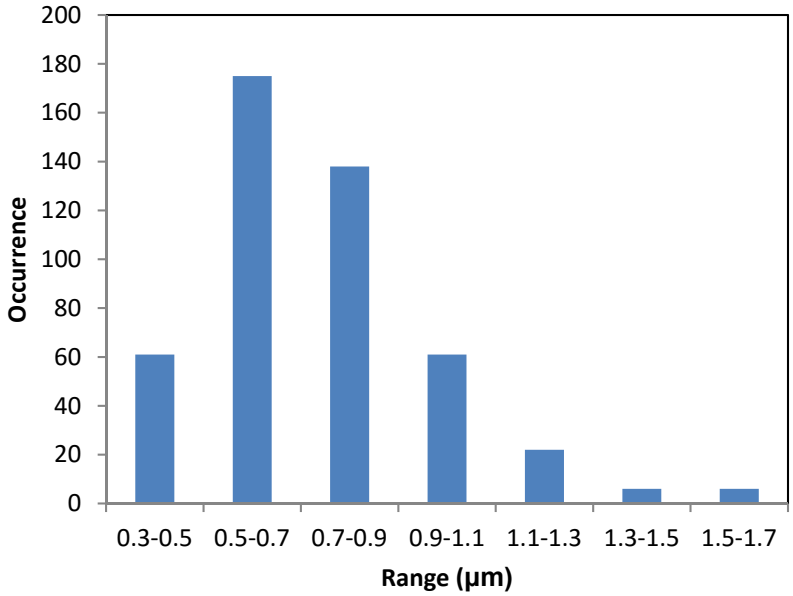

(c)

Fig. 4. (a,b) Fine basketweave microstructure in Ti-5Al-5Mo-5V-1Cr-1Fe titanium alloy, by SEM; (c) histogram of width of α plates inside grains.

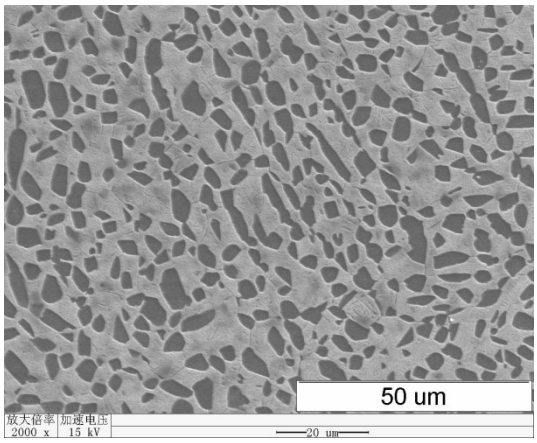

(a)

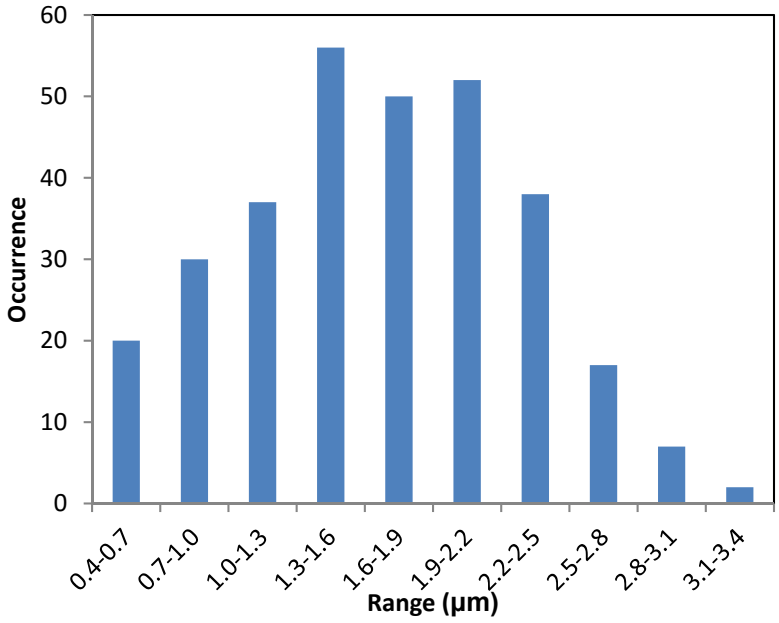

(b)

Fig. 5. (a) Coarse basketweave microstructure in Ti-5Al-5Mo-5V-1Cr-1Fe titanium alloy, by low magnification SEM; (b) α phase dimension histogram.

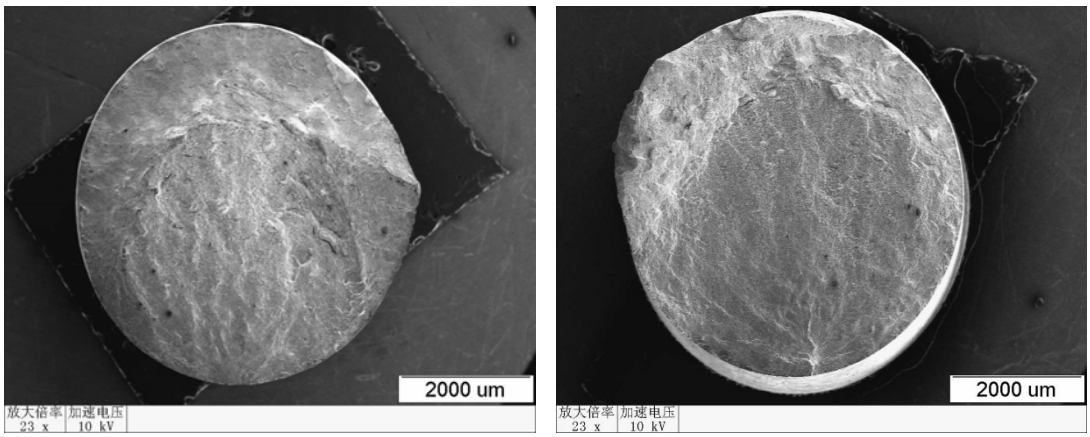

(a) (b)

Fig. 6. SEM macroscopic images of high cycle fatigue fracture surfaces of Ti-5Al-5Mo-5V-1Cr-1Fe titanium alloy having a coarse basketweave structure. (a) Load 875 MPa, life 9.6×10^4; (b) load 625 MPa, life 9.1×10^6.

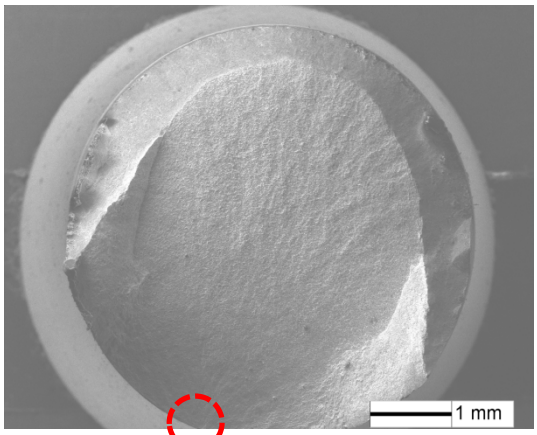

(a)

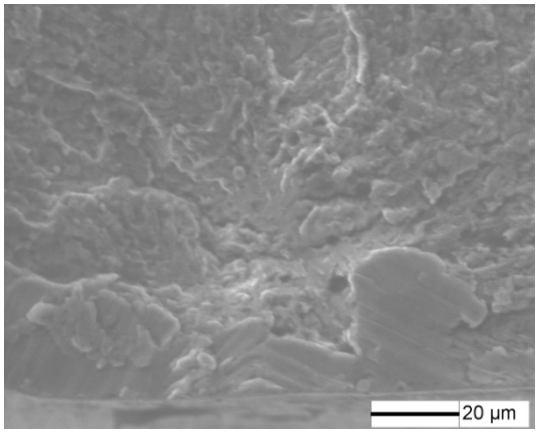

(b)

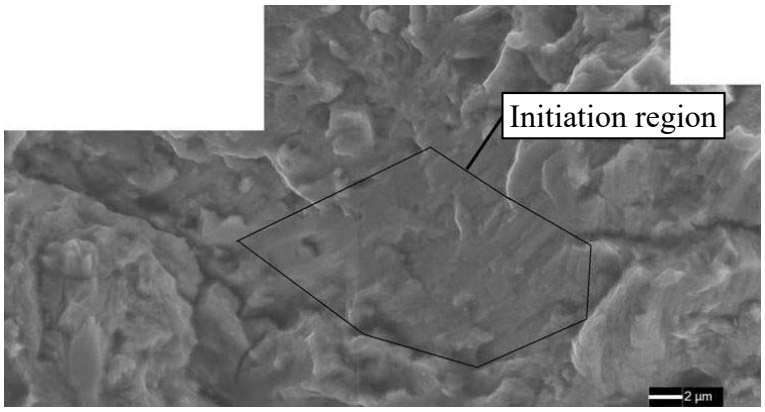

(c)

Fig. 7. SEM images of high cycle fatigue fracture surface of Ti-5Al-5Mo-5V-1Cr-1Fe titanium alloy having a bimodal structure. (a) Macroscopic fracture surface, where crack initiation site is marked with a dashed circle; (b,c) fracture initiation area.

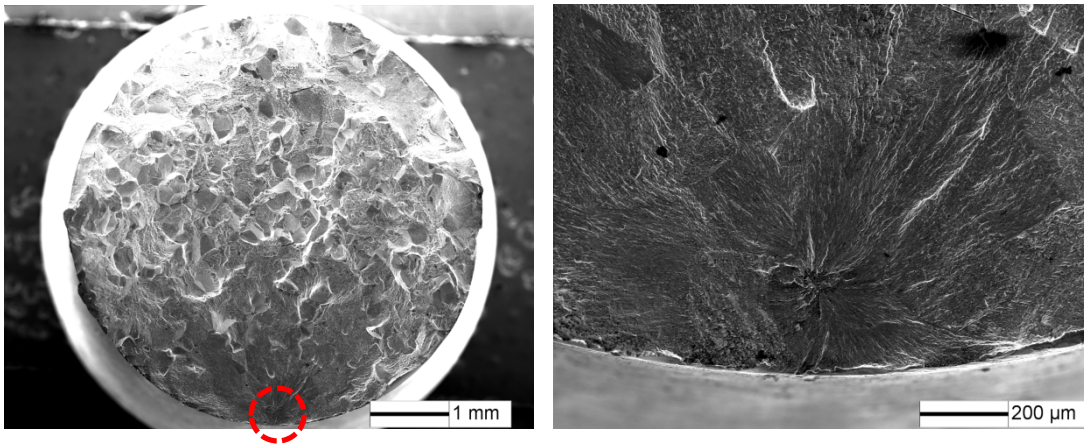

(a) (b)

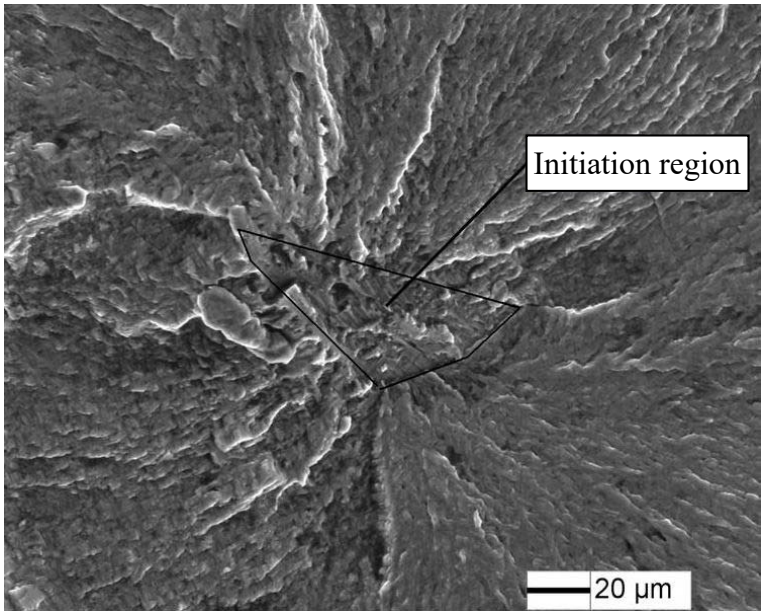

(c)

Fig. 8. SEM images of high cycle fatigue fracture surface of Ti-5Al-5Mo-5V-1Cr-1Fe titanium alloy having a Widmanstätten structure. (a) Macroscopic fracture surface, where crack initiation site is marked with a dashed circle; (b,c) fracture initiation area.

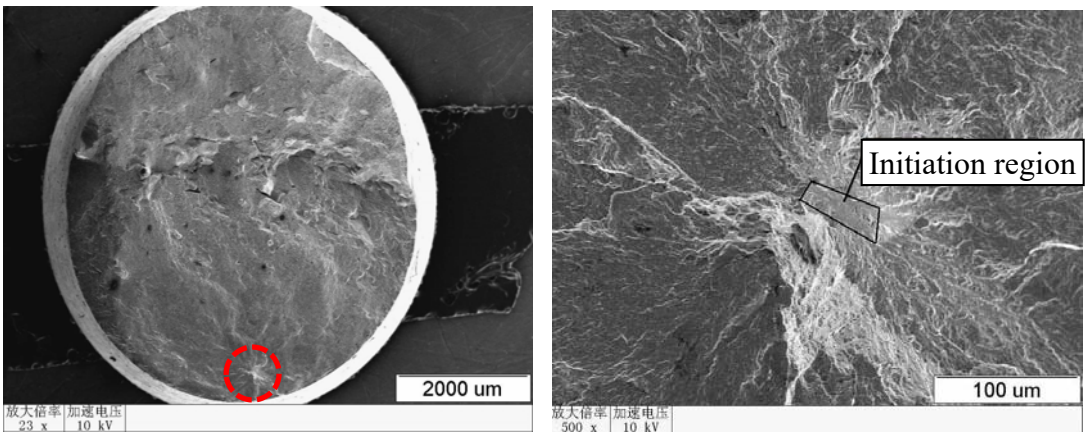

(a) (b)

Fig. 9. SEM images of high cycle fatigue fracture surface of Ti-5Al-5Mo-5V-1Cr-1Fe titanium alloy having a fine basketweave structure. (a) Macroscopic fracture surface, where crack initiation site is marked with a dashed circle; (b) fracture initiation area.

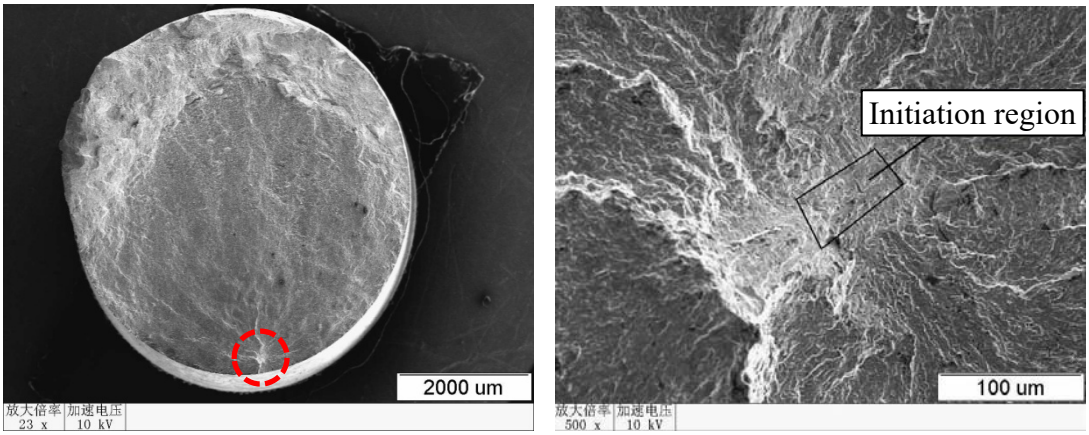

(a) (b)

Fig. 10. SEM images of high cycle fatigue fracture surface of Ti-5Al-5Mo-5V-1Cr-1Fe titanium alloy having a coarse basketweave structure. (a) Macroscopic fracture surface, where crack initiation site is marked with a dashed circle; (b) fracture initiation area.

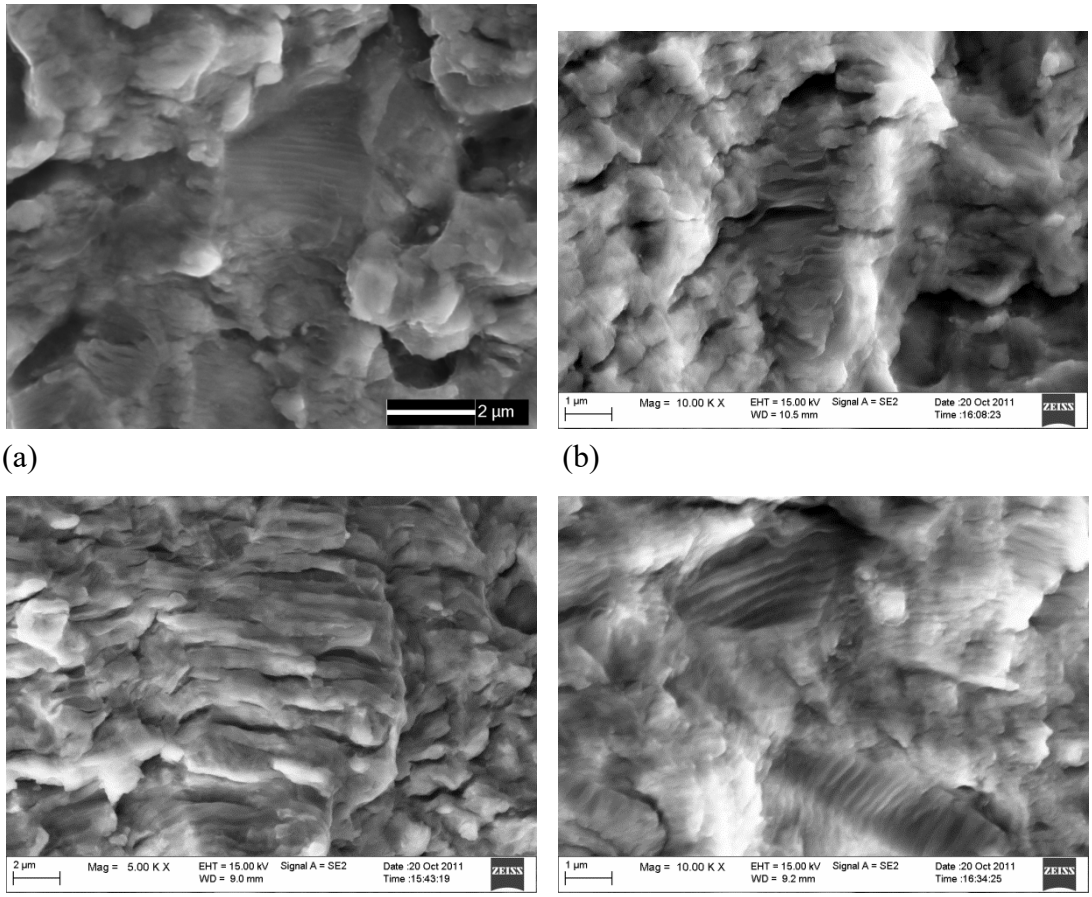

(a) (b)

(c) (d)

Fig. 11. SEM images showing morphology characteristics of stable propagation region in high cycle fatigue fracture surfaces of Ti-5Al-5Mo-5V-1Cr-1Fe titanium alloy having different microstructure types. (a) Bimodal; (b) Widmanstätten; (c) fine basketweave; (d) coarse basketweave.